JASA ARTICLE

Observations of acoustic noise bursts accompanying nonlinear internal gravity waves on the continental shelf off New Jersey

Boris G. Katsnelson,[1,a)] Oleg A. Godin,[2,b)] and Qianchu Zhang[1,c)]
[1]*Department of Marine Geosciences, University of Haifa, Haifa 3498838, Israel*
[2]*Physics Department, Naval Postgraduate School, Monterey, California 93943, USA*

ABSTRACT:
Anomalously large, transient fluctuations of acoustical noise intensity, up to 4–5 orders of magnitude above the background, were observed with single-hydrophone receiver units (SHRUs) and on the L-shaped horizontal and vertical line array of hydrophones (HVLA) in the Shallow Water 2006 experiment on the continental shelf off New Jersey. Here, temporal and spatial properties of these noise bursts are investigated. As tidally generated nonlinear internal waves (NIWs) move across the site of the experiment from the shelf break toward the coast, they form trains of localized, soliton-like waves with up to 25–35 m displacement of isopycnal surfaces. The NIW trains consecutively cross the positions of five SHRUs and HVLA that are located about 5–8 km from each other along a line perpendicular to the coast. The noise bursts were observed when a NIW train passed through locations of the corresponding acoustic receivers. Turbulence of the water flow, saltation, and bedload of marine sediments were the dominant causes of the acoustic noise bursts caused by NIWs at different frequency bands. On near-bottom hydrophones, the most energetic part of the observed noise bursts is attributed to collisions of suspended sediment particles with each other, the sensor, and the seafloor. © *2021 Acoustical Society of America.*
https://doi.org/10.1121/10.0003624
(Received 29 November 2020; revised 4 February 2021; accepted 12 February 2021; published online 9 March 2021)
[Editor: D. Benjamin Reeder] Pages: 1609–1622

I. INTRODUCTION

Internal gravity waves in the ocean create time-dependent and spatially inhomogeneous variations in temperature and sound speed profiles and are known to have a significant effect on underwater sound propagation (Simmen *et al.*, 1997; Colosi *et al.*, 1999; Tang *et al.*, 2007). Especially strong variations in the sound propagation conditions and attendant fluctuations of the acoustic fields occur due to nonlinear internal waves (NIWs) on continental shelves (Zhou *et al.*, 1991; Godin *et al.*, 2006; Apel *et al.*, 2007). The magnitude of the acoustic effects depends on the NIW amplitude and spatial structure as well as on the azimuthal direction of the acoustical track relative to the direction of NIW propagation, which determines the dominant physical mechanism of the NIW-sound interaction. For example, on a 14 km propagation track largely along NIW wavefronts in the SWARM95 experiment in the Mid-Atlantic Bight, NIW-induced focusing and defocusing of acoustic normal modes in the horizontal plane was found to result in sound intensity fluctuations of low-frequency signal (20–300 Hz), with magnitudes of 7–8 dB and periods of about 10 min (Badiey *et al.*, 2002, 2007). In the same experiment, for mid-frequency signals (a few kHz) on a different sound propagation track crossing the NIW wavefronts, sound intensity fluctuations of a few dB took place due to NIW-induced coupling of the acoustic normal modes (Badiey *et al.*, 2002; Katsnelson *et al.*, 2009). Perhaps the strongest reported NIW-induced fluctuations of the transmission loss, or frequency-dependent sound intensity, of 20–25 dB were observed in the Yellow Sea off China; these were explained in terms of the resonant Bragg scattering of sound by a NIW wave train (Zhou *et al.*, 1991; Apel *et al.*, 2007).

In addition to the propagation effects, NIWs were observed to change sound intensity by generating underwater acoustic noise. Currents of various nature, including NIW-induced currents, shed vortices and generate turbulent pressure fluctuations when flowing past acoustic sensors and elements of their moorings. These pressure fluctuations are observed as very low-frequency noise (typically, below a few tens of Hertz) and are known as flow noise (Strasberg, 1979; Webb, 1988). Measurements of NIW-induced flow noise have been described in the literature (Serebryany *et al.*, 2008a; Yang *et al.*, 2013). At higher frequencies, Serebryany *et al.* (2005, 2008a, 2008b) observed strong fluctuations of the ocean surface-generated broadband acoustic noise that accompanied passage of a strong NIW. These fluctuations were attributed to the modulation of the surface gravity and capillary-gravity wave activity on the ocean surface by NIW-induced currents. NIW-induced fluctuations of the intensity of the surface-generated noise reached 10–15 dB in deep water in the Indian Ocean (Serebryany *et al.*, 2005) and up to about 6 dB on the continental shelf in the

[a)]Electronic mail: bkatsnels@univ.haifa.ac.il, ORCID: 0000-0001-8934-5504.
[b)]ORCID: 0000-0003-4599-2149.
[c)]ORCID: 0000-0003-0556-0915.

Mid-Atlantic Bight (Serebryany *et al.*, 2008a). Similar observations were made by Yang *et al.* in the Pacific northeast of Taiwan (Yang *et al.*, 2013) and in the South China Sea (Yang *et al.*, 2015), with about 10 dB variations of the acoustic noise intensity due to NIW-induced changes in the surface wave activity.

In the present paper, we describe our analysis of observations of very large (up to 50 dB) broadband, transient increases in the noise intensity, to be referred to as noise bursts, on the continental shelf off New Jersey. By combining acoustic observations on various hydrophones with measurements of the water temperature and current velocity, we established a relationship between individual noise bursts and tidally generated, localized, soliton-like NIWs and identified the physical mechanisms likely responsible for the observed acoustic manifestations of the NIWs.

The paper is organized as follows. Section II outlines acquisition of the data used in this study. Properties of the noise bursts are discussed in Sec. III. In Sec. IV, we show that the observed temporal and spectral characteristics of the noise bursts can be explained in terms of three physical mechanisms of noise generation, which include turbulence of the water flow and NIW-induced sediment saltation. Section V puts our findings into the broader context of previous research on sediment-generated underwater noise (SGN) and sediment resuspension by NIWs. The results of the work are summarized in Sec. VI along with their possible application to investigation of soliton-like NIWs and of contributions of the NIWs to the sediment transport on the continental shelf.

II. EXPERIMENT AND DATA

The data used in this study were obtained in the multidisciplinary, multi-institutional Shallow Water 2006 experiment (SW'06). The experiment was carried out in July to September of 2006, in the Mid-Atlantic Bight on the continental shelf off New Jersey (Newhall *et al.*, 2007; Tang *et al.*, 2007; Lynch and Tang, 2008; Xue *et al.*, 2014). A bathymetric map of the experiment site is shown in the lower left corner of Fig. 1. Water depth in this area decreases gradually from about 120 m near the shelf break to 55–60 m 40 km from the shelf break. The typical summer water temperature profile was characterized by a monotonic temperature decrease from the surface to the seafloor and a rather strong thermocline with about 12 °C temperature drop between 10 and 25 m depths. The corresponding sound speed profile was at its minimum on the seafloor and provided for a bottom-interacting guided sound propagation. However, occasional near-bottom intrusions of warm, salty water, sometimes referred to as "the foot of the shelfbreak front" (Linder and Gawarkiewicz, 1998), raised the sound speed minimum to as high as the middle of the water column on some days during the observation period (Newhall *et al.*, 2012).

The site of the experiment is characterized by a strong internal gravity wave activity, which is well-documented (Tang *et al.*, 2007; Shroyer *et al.*, 2011; Xue *et al.*, 2014). Approximately twice a day, a strong NIW is generated around the shelf break as a result of interaction of barotropic tides with the bathymetry. NIWs move from the shelf break shoreward in the northwest direction, largely along the bathymetry gradient. Over the 2-month duration of the

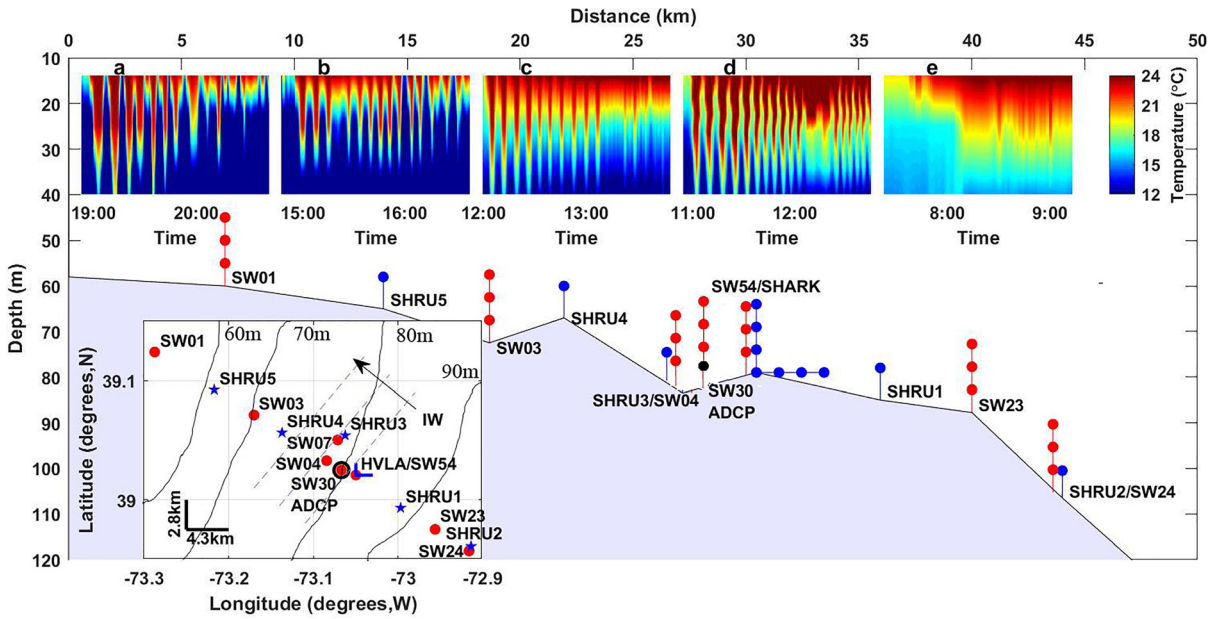

FIG. 1. (Color online) Evolution of a train of NIWs over the site of the SW'06 experiment. Positions of thermistor chains SW01, SW03, SW04, SW07, SW23, SW24, SW30, and SW54; single-hydrophone acoustic receivers SHRU1, SHRU2, SHRU3, SHRU4, and SHRU5; and hydrophone array HVLA Shark as well as wave fronts (dashed lines) and the direction of propagation (arrow) of an internal wave train are indicated in the map in the lower left corner. Bathymetry is shown along the straight line through SW01 and SW24. ADCP is located at SW30. Depth dependence of water temperature as measured by SW01 (a), SW03 (b), SW04 (c), SW54 (d), and SW23 (e) is shown from 07:00 to 21:00 GMT on 19 August 2006 when a train of NIWs propagated shoreward from SW23 past SW01. Time (GMT) on 19 August 2006 is shown in hours and minutes.

https://doi.org/10.1121/10.0003624

experiment, tens of events were registered of NIW train passages through the instrumented site. Direction of propagation and surface structure (shape of wavefronts, the number of waves in the train, and distance between them) were obtained using shipboard observations (Shroyer *et al.*, 2011) and satellite images (Xue *et al.*, 2014), which show a rather narrow spread of NIW propagation directions in the horizontal plane. NIW propagation directions were nearly parallel to the across-shelf line, along which a suite of acoustic sensors, thermistor chains, and acoustic Doppler current profilers (ADCPs) was deployed (Fig. 1).

Detailed information about the three-dimensional structure and temporal evolution of the NIW trains was obtained using a few tens of thermistor chains (Newhall *et al.*, 2007; Tang *et al.*, 2007; Lynch and Tang, 2008; Shroyer *et al.*, 2011). These data show that the NIWs were predominantly depression waves except for possible reversal of polarity at shoaling that was observed (Shroyer *et al.*, 2009) on several occasions. As the semidiurnal internal tide moved from the shelf break toward the shore, each tidal internal wave evolved into a wave train consisting of up to 10–12 localized, soliton-like waves (Fig. 1). The isopycnal depression amplitude of the individual localized waves was largest near the leading front of the train and gradually decreased toward its back end. The observed wave trains were qualitatively similar to the D-noidal model of NIWs (Apel, 2003).

Observations of strong NIW events on 17, 18, 19, and 22 August 2006 have been selected for the present study. These events had quite similar patterns of NIW movement and, in turn, similar features of acoustic intensity fluctuations. Consider a 12-h time period from 08:00 to 20:00 GMT on 19 August 2006. The period started with the appearance of a NIW in the shelf-break area. The NIW evolution process can be analyzed using temperature records from a cluster of 16 thermistor chains in a $2 \times 2\,\mathrm{km}^2$ square-shaped area (Newhall *et al.*, 2007). Temperature was sampled at 30 s intervals. Positions of selected thermistor chains, denoted by the letters SW, and of the acoustic receiving systems, single-hydrophone receiving units (SHRUs) and the L-shaped horizontal and vertical line hydrophone array (HVLA) Shark, are shown on the bathymetric map in Fig. 1. SHRUs were moored with heavy anchors, with the hydrophone located about 7 m above the seafloor. HVLA Shark consisted of a 16-hydrophone vertical linear array (VLA), which extended through most of the water column, and a 450-m-long, 32-hydrophone, near-bottom horizontal linear array (HLA).

Five panels at the top of Fig. 1 show the temperature records obtained by five thermistor chains located at various distances from the shelf break. Each temperature record was 90 min long, corresponding to the time it took a NIW train to pass each thermistor chain. It can be seen that the NIW train was generated in the area between SW23 (where we can see the forward front of an unstructured NIW) and SW54, where the NIW had developed a well-defined across-the-front structure. The distance between SW23 and SW24 was about 14 km. At SW54, the NIW contained 12 distinct, soliton-like waves (peaks of the depression of the isothermal surfaces) with amplitudes of the thermocline's displacement from equilibrium position of up to 25–30 m (Fig. 1). As the NIW train moved shoreward, it passed consecutively a set of acoustic receivers, including the HVLA Shark and five SHRUs, which were located a distance of 5–8 km from one other along a straight line. The NIW train evolved as it propagated; the amplitudes and the number of the localized waves in the train changed (Fig. 1). One can estimate the speed v of the NIW train using the distance between thermistor chains and the temporal interval between arrivals of the NIW leading front. From such an estimate, we obtained $v \sim 0.9$ m/s, length of the NIW trains $L \sim 5$ km, and quasi-period of the spatial structure inside the NIW train $l \sim$ 250–300 m. The corresponding scale of temporal variability was 5–7 min.

For the entire duration of the SW'06 experiment, acoustic pressure was continuously measured by the SHRU and HVLA Shark hydrophones. The acoustic data were recorded with a common sampling rate of 9765.625 Hz for all hydrophones. Measured time series $p(t)$ of acoustic pressure p are used below for calculation of various characteristics of the acoustic field, including its intensity, frequency spectrum, and spectrograms. In addition, current velocity was measured using ADCPs. The data obtained with a moored 300 kHz ADCP (Fig. 1) that was used in this study are described in Sec. III.

III. OBSERVATIONS OF NOISE BURSTS

The vertical line array of HVLA Shark was collocated with thermistor chain SW54 (Fig. 1), but other acoustic receivers, including SHRU1, SHRU4, and SHRU5, had no collocated temperature sensors. Figure 2 presents a diagram demonstrating the connection between NIW passage and observations of elevated noise intensity at different points across the shelf. In the top panel, the vertical axis denotes distance along the straight line through locations of the hydrophones and thermistor chains, with 0 of this axis corresponding to the position of the thermistor chain SW01. The horizontal axis represents time and covers 15 h of observations. Temporal variation of temperature at different locations is illustrated by temperature measurements (denoted by the letter t), by one thermistor at 40 m depth of each of five thermistor chains. Note that all positions of the forward front of the NIW train in the range-time plane were located approximately along a straight line, which indicates a nearly constant speed of the NIW train of 0.9 m/s. Time series of measured sound intensity are shown for four SHRUs and one of the hydrophones (channel 40) of HVLA Shark. The parts of these records that show large, rapid increases (bursts) of the noise intensity are indicated by boxes (a)–(e). Figure 2 shows that the noise bursts were observed when the NIW train traveled past the acoustic sensor.

More detailed information about the frequency content of acoustic signals and its time dependence can be obtained

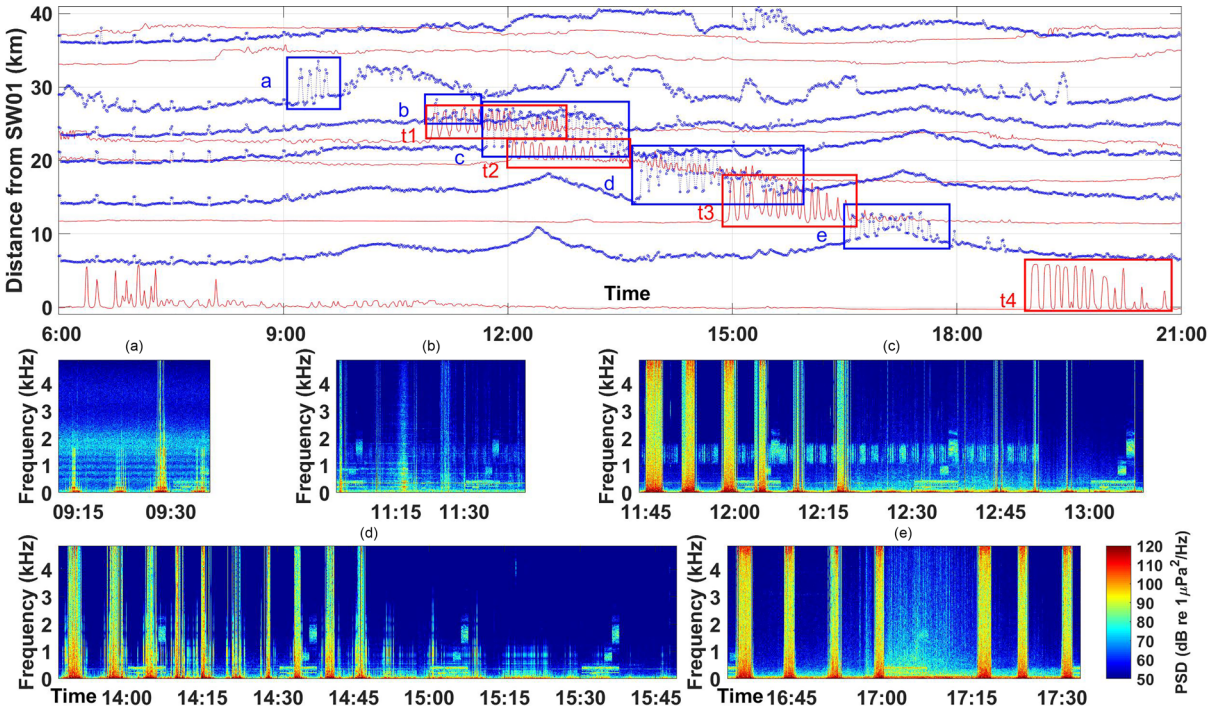

FIG. 2. (Color online) Time histories of water temperature and acoustic intensity at various points along the path of propagating internal wave train. Temperature records of thermistors at the depth of 40 m are denoted by the letter T and depicted in red for thermistor chains SW23, SW54, SW04, SW03, and SW01. Time intervals of appearance of the NIW train are denoted t1, t2, t3, and t4 for the last four chains (SW23 does not show NIWs) and boxed. Sound intensity records by SHRU1, SHRU3, SHRU4, and SHRU5 and hydrophone 40 of HVLA Shark are depicted in blue. For visibility, the time dependences recorded by individual sensors are shifted vertically in proportion to the distance from the sensor to SW01. Time intervals with strong fluctuations of acoustic pressure are boxed and marked for SHRU1 (a), HVLA Shark (b), SHRU3 (c), SHRU4 (d), and SHRU5 (e). Time (GMT) on 19 August 2006 is shown in hours and minutes. (a)–(e) Five color panels in the lower part of the figure show the spectrograms corresponding to the sound intensity records in boxes a–e.

using spectrograms. Spectrograms $S(f, t)$ have been calculated in the frequency range 10–4000 Hz as follows:

$$S(f, t_1) = \int W(t - t_1) p(t) e^{-i2\pi ft} dt. \quad (1)$$

Here $p(t)$ is a measured time series of acoustic pressure, f is sound frequency, and $W(t–t_1)$ is the time window. A Kaiser window (Kaiser and Schafer, 1980) incorporating 1024 pressure samples was used. Figure 2 shows spectrograms of noise recorded when a NIW train was moving consecutively through positions of SHRU1 [Fig. 2(a)]; HVLA Shark [channel 40, hydrophone in the center of HLA, Fig. 2(b)]; and SHRU3, SHRU4, and SHRU5 [Figs. 2(c), 2(d), and 2(e), respectively]. HVLA Shark is represented in Fig. 2 by measurements on channel 40, which was a hydrophone at the center of the horizontal line array.

In the area of NIW generation, where water depth was about 100 m, fluctuations of acoustic intensity were relatively weak, especially at frequencies above 1 kHz [see Fig. 2(a)], although there was some correlation of the intensity fluctuations with NIWs. In particular, the temporal scale of the sound variability of about 7 min corresponded to the time interval between separate localized waves with the NIW train. A similar situation took place on the HVLA Shark hydrophones [Fig. 2(b)]. Noise intensity was significantly weaker on the vertical part of the L-shaped array than on its horizontal part, as was previously reported by Serebryany *et al.* (2008a).

Acoustic intensity fluctuations increased as the NIW train moved to shallower water. Figure 2(d) depicts the spectrogram of noise recorded by SHRU4, which was located between thermistor chains SW03 and SW04. Comparison of the shapes of the NIW train recorded by these thermistor chains [Figs. 1(b) and 1(c)] shows that the main parameters of the NIW train—the number of individual localized waves, their amplitudes (~30–40 m), and the time interval between the waves (~7 min)—did not change significantly between SW03 and SW04. Hence, SW03 and SW04 measurements should provide a suitable representation of the NIW train at SHRU4. Comparison of the temperature record in Fig. 1(c) and spectrogram in Fig. 2(d) demonstrated a good agreement between the temporal scales (total duration of about 1 h, the interval between peaks ~ 7 min) in the temperature and intensity measurements. The agreement between time dependences of the temperature variations and acoustic spectra indicated a causal relation between NIWs and noise intensity fluctuations at SHRU4 and, by extension, at other locations on the continental shelf.

The SW3 and SW4 temperature records [Figs. 1(b) and 1(c)] have 12 large peaks, which corresponded to individual localized internal waves. Amplitude of the waves tended to decrease toward the tail of the NIW train. The data from acoustic sensors SHRU3 and SHRU4, which were located

https://doi.org/10.1121/10.0003624

between the thermistor chains SW3 and SW4 (Fig. 1), showed fewer peaks in the spectrograms. There are six strong, broadband noise bursts in SHRU3 data in Fig. 2(c). Water depth was about 68 and 82 m at SHRU4 and SHRU3 locations, respectively. For SHRU4, which was located in shallower water of 68 m depth, Fig. 2(d) shows 10 strong, broadband noise bursts. We relate the observed difference in the number of noise bursts to the difference in the speed of the near-bottom currents induced by NIWs at the two sites. As discussed in Sec. IV, speed of the near-bottom currents increased with increasing wave amplitude and decreasing water depth [see Eq. (4)]. The change in the number of noise bursts at frequencies above a few hundred Hertz suggests that acoustic noise generation has a threshold character. Number of noise bursts is equal to number of the individual localized peaks in the NIW train with the speed of near-bottom current larger than threshold value.

The value of the threshold can be estimated by combining the noise intensity and water temperature measurements with current velocity data. Current velocity was not measured at acoustic sensor locations. We used the velocity data obtained with an ADCP, which was collocated with the thermistor chain SW30. Figure 3 compares the ADCP measurements with simultaneous measurements of the water temperature profile by thermistor chains SW07 and SW30 and acoustic observations at SHRU3. In the direction across the NIW wavefront, SW30 and ADCP preceded SHRU3 by about 700 m, and SW07 was behind SHRU3 by about 500 m (Fig. 1). This geometry was responsible for the 10–15 min shifts of the respective temperature and current velocity manifestations of a NIW wave train [Figs. 3(b)–3(d)] from its acoustic manifestations [Fig. 3(a)]. The wave train evolved as it propagated. Isothermal depressions had five and seven strong peaks following the leading front of the NIW train at SW07 and at SW30, respectively [Figs. 3(b) and 3(c)]. It is reasonable to assume that there were six strong peaks at SHRU3, which is located between SW07 and at SW30. Figure 3(a) shows six strong, broadband noise bursts following the leading front of the NIW train.

Horizontal velocity of the water flow caused by the NIW train reached its maximum when the isothermal depression was at maximum [Figs. 3(c) and 3(d)]. Observed velocities reached—and for the strongest peaks exceeded—60 cm/s below the thermocline. Velocity magnitude gradually declined with depth below the thermocline and decreased by a factor of about 1.5 near the bottom [Fig. 3(d)]. Comparison of the spectrogram of acoustic noise with the ADCP measurements indicated that strong, broadband noise bursts occurred when the NIW-induced near-bottom current exceeded a threshold value of about 40 cm/s.

These results suggest that the noise bursts occurred around the time when a peak of isothermal depression passed the observation point. A more precise relation between the phase of the isothermal displacement and acoustic noise can be obtained using the HVLA Shark data, since SW54 thermistors were attached to the vertical part of the hydrophone array. Figure 4 compares simultaneous, collocated measurements of the water temperature profile and

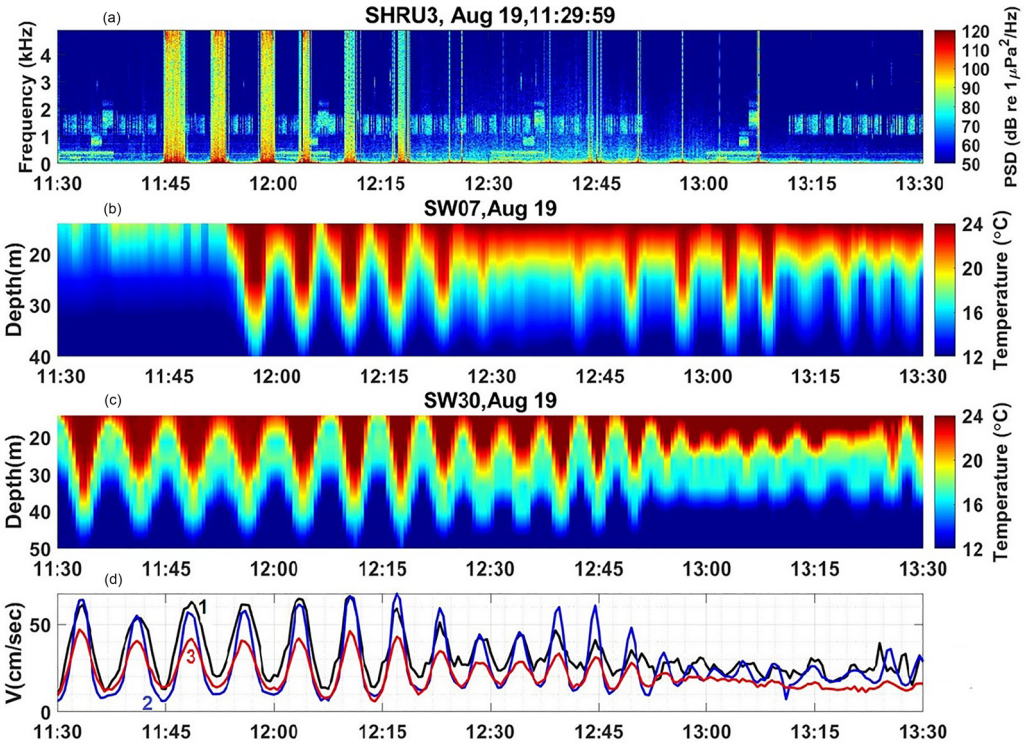

FIG. 3. (Color online) Temperature, current velocity, and acoustic manifestations of a NIW train in the vicinity of the acoustic receiver SHRU3. (a) Spectrogram of acoustic noise recorded by SHRU3. (b) Time history of the water temperature on the thermistor chain SW07. (c) Time history of the water temperature on the thermistor chain SW30. (d) Time dependence of the horizontal current velocity at three depths: 20.2, 44.2, and 68.2 m. Time (GMT) on 19 August 2006 is shown in hours and minutes.

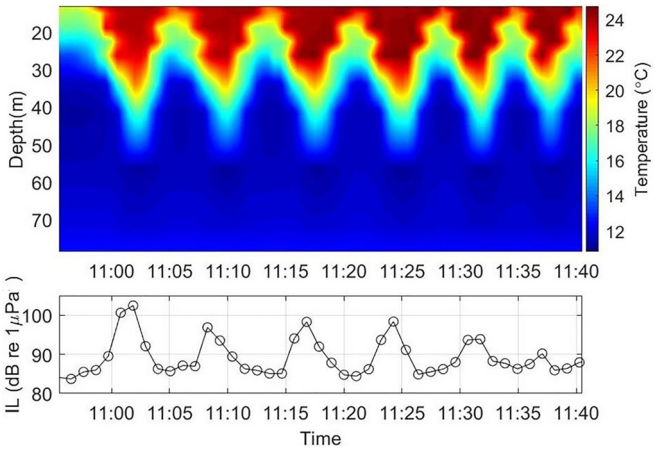

FIG. 4. (Color online) Temporal variations of the temperature depth dependence measured by thermistor chain SW54 (upper panel) and noise intensity on a collocated hydrophone (lower panel). Time (GMT) on 19 August 2006 is shown in hours and minutes.

sound intensity on the lowest hydrophone on the vertical part of the array. The figure demonstrates that maximum noise intensity was observed when the NIW-induced displacement of isothermal surface was at maximum. The time-dependent acoustic intensity I and intensity level IL were calculated as follows:

$$I(t_1) = \frac{1}{2\rho c \Delta t}\int_{t_1}^{t_1+\Delta t} |p(t)|^2 dt, \tag{2}$$

$$IL(t_1) = 10\log_{10}\left[\frac{I(t_1)}{I_0}\right]. \tag{3}$$

Here $\Delta t = 1$ s is the averaging time, ρ and c are the density and sound speed in water, and I_0 is the reference intensity, corresponding to the root mean square acoustic pressure of 1 μPa.

The noise generated by NIWs on near-bottom hydrophones was as strong as, if not stronger than, any signal received or noise of a different origin. This is illustrated in Fig. 5, which shows the time dependence of acoustic intensity recorded by SHRU5 during a full day. A number of sound generation mechanisms contributed to the observed acoustic field. For instance, from 04:00 to 17:00 there were prominent signals from the research sources (Newhall *et al.*, 2007; Lynch and Tang, 2008), which were towed through the experiment site. Strong low-frequency noise, presumably due to shipping and/or a storm, was present from about 10:00 to 14:00. This noise was superimposed on and overshadows signals from the research sources. NIW-induced noise intensity bursts appeared as a sequence of high and narrow, quasi-periodic intensity peaks in the 16:30–17:30 time interval. Intensity of the noise bursts reached 150–155 dB re 1 μPa. It exceeded the background noise intensity of 110–115 dB re 1 μPa by 40 dB, or 4 orders of magnitude.

IV. MECHANISMS OF NOISE GENERATION

Noise intensity, its time dependence, and the spectral content of the noise showed significant variability, depending on hydrophone position and position of NIW train. Three distinct types of acoustic noise that accompanied the passage of NIWs can be identified, which combined to explain the bulk of observations (see Fig. 6). These types are (i) low-frequency noise, which is illustrated in Figs. 6(a) and 6(b); (ii) noise spikes of ~1 s duration with spectral peaks located below approximately 1 kHz [Fig. 6(c)]; and (iii) more frequent, shorter-duration spikes with prominent high-frequency content above 3 kHz, which subsequently merged to become a continuous signal of a few minutes in duration [Fig. 6(d)].

The low-frequency noise was most pronounced at infrasonic frequencies below 10 Hz [Fig. 6(b)]. It was observed almost continuously as each soliton-like wave in the NIW train passed the acoustic receiver. Acoustic intensity increased rapidly with the magnitude of pycnocline depression [see the time dependence of noise spectral density at frequencies below 10 Hz in Fig. 6(b)]. The low-frequency noise was clearly observed on all SHRUs and on VLA hydrophones, where noise intensity was only weakly dependent on the hydrophone depth.

We interpret the low-frequency noise that was observed as flow noise (Strasberg, 1979; Webb, 1988; Bassett *et al.*, 2014). Flow noise, also known as pseudosound, results from advection of pressure fluctuations in a turbulent flow past the sensor. Pressure fluctuations include ambient fluctuations in a turbulent flow as well as pressure pulsations due to eddy shedding when the flow interacts with the sensor and the entire mooring. Intensity of flow noise is known to increase with decreasing frequency (Strasberg, 1979; Webb, 1988; Bassett *et al.*, 2014). Interpretation of the low-

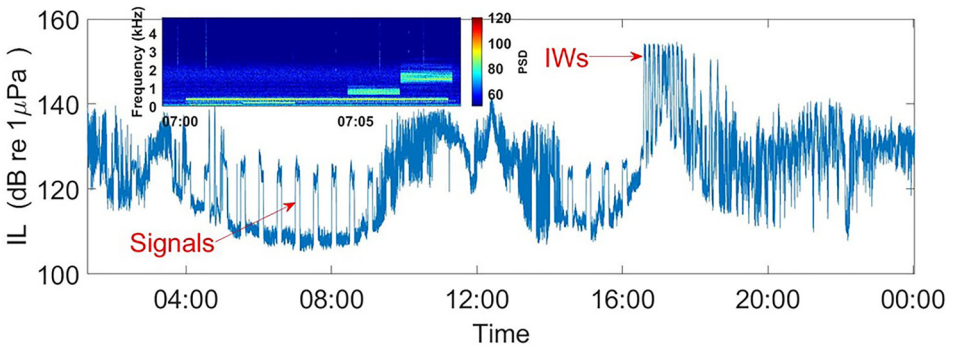

FIG. 5. (Color online) Temporal variation of the acoustic intensity measured by SHRU5. Time (GMT) on 19 August 2006 is shown in hours and minutes. The inset shows the spectrogram of a 9-min section of the pressure record and illustrates contributions of research sound sources. Color shows power spectral density of total acoustic field in dB re 1 μPa^2/Hz.

https://doi.org/10.1121/10.0003624

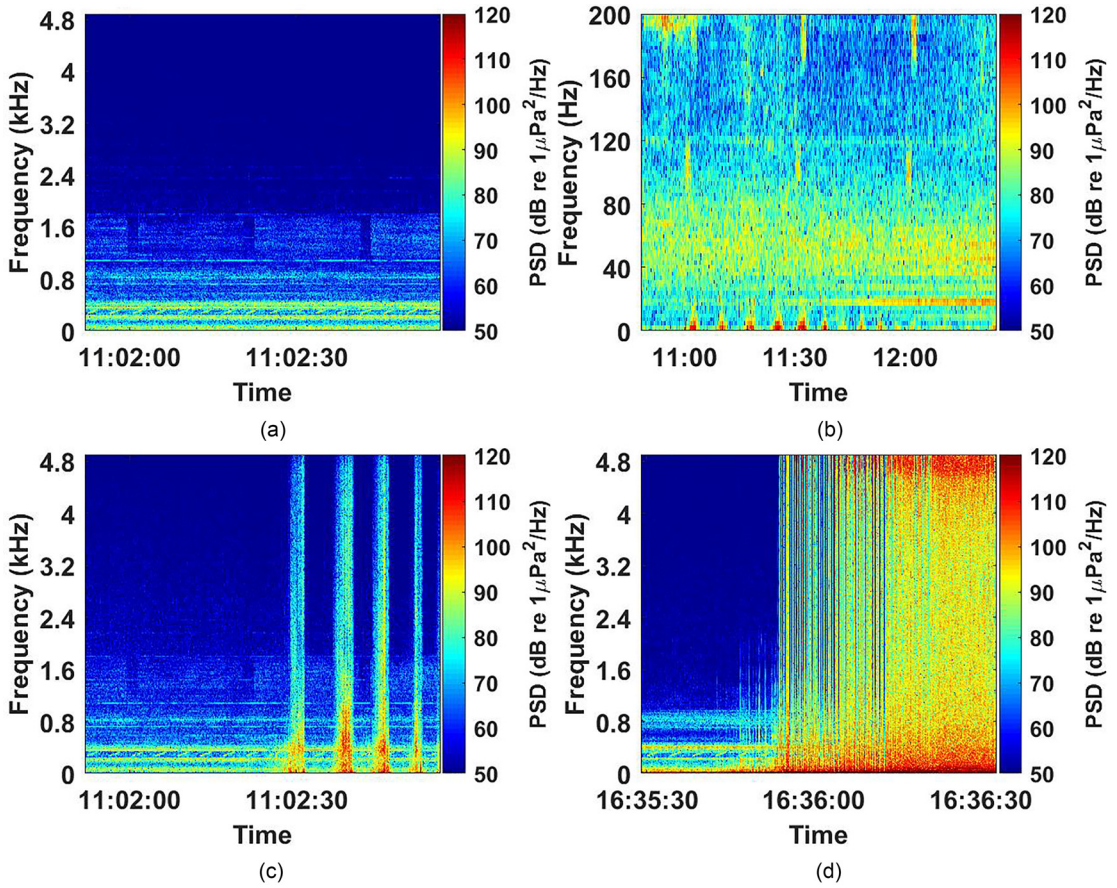

FIG. 6. (Color online) Spectrograms of the acoustic field recorded by hydrophones on vertical and horizontal line arrays and a single hydrophone receiver during passage of a train of NIWs. Spectrograms are shown of acoustic pressure on a VLA hydrophone at a depth of 62 m (a); the low-frequency part of the acoustic pressure on the same hydrophone (b); acoustic pressure on a hydrophone in the middle of HLA (c); and acoustic pressure on single-hydrophone receiver SHRU5 (d). Time (GMT) on 19 August 2006 is shown in hours minutes, and seconds.

frequency noise as flow noise is supported by the apparent absence of such noise in signals on HLA hydrophones, which lie on the seafloor. For the pseudosound due to eddy shedding, by the flow past a cylinder of diameter d, the representative frequency is $f_e = St\ u/d$, where $St \sim 0.2$ is the Strouhal number and u is flow velocity (Strasberg, 1979; Webb, 1988). With NIW-induced currents of ~0.5 m/s [Serebryany *et al.*, 2008a; see also Fig. 3(d)], the observed upper frequency of 10 Hz is consistent with the eddy shedding by a mooring wire with $d \sim 1$ cm. The hydrophone and pressure housing have larger dimensions and contribute to lower-frequency pseudosound.

The observed strong correlation between intensity of low-frequency noise and pycnocline depression in NIWs (Fig. 4) can be understood within the following simple model of NIW currents. Consider a progressive NIW with a linear wavefront, which moves with speed c along horizontal coordinate x in an ocean, where potential density jumps across a narrow pycnocline and remains constant below it. Let the water depth, unperturbed pycnocline depth, and pycnocline depression due to NIW be $H(x)$, $h(x)$, and $\eta(x - ct)$. The flow is stationary in the reference frame moving with NIW. In the long-wave approximation (Apel *et al.*, 2007), it follows then from the continuity equation that flow velocity $u(x, t)$ below the pycnocline is

$$u = \frac{-c\eta(x - ct)}{H(x) - h(x) - \eta(x - ct)}. \tag{4}$$

The minus sign in the numerator in Eq. (4) indicates that near the seafloor, water flows in the direction opposite to the direction of NIW propagation. Note that magnitude $|u|$ of the flow velocity rapidly increases with increasing pycnocline depression and, for fixed η, is inversely proportional to the distance from the perturbed pycnocline to the seafloor. For example, in the vicinity of SHRU3, the water depth was $H \approx 80$ m, thickness of thermocline $h \approx 20$ m, and the pycnocline depression $\eta \approx 20$ m, and Eq. (4) gives $|u| = c/2 \sim 0.5$ m/s. This estimate agrees well with the ADCP measurements shown in Fig. 3(d).

The key to understanding the origin of the second noise type, illustrated in Fig. 6(c), is the fact that it was observed only on HLA hydrophones and was not present on either VLA hydrophones or SHRUs. HLA hydrophones lay on the seafloor, while the VLA and SHRU hydrophones were located at least 6 m above it. Moreover, the type-two noise was at maximum on hydrophones in the middle of the HLA,

and no noise of this type was observed on the hydrophones at both ends of the array, which were fixed by heavy anchors (Newhall *et al.*, 2007). All the observed features of type-two noise are consistent with hydrophones being dragged along the seafloor by NIW-induced near-bottom currents, with the stronger noise caused by the bigger displacements that occurred away from the anchors. This interpretation was proposed by Serebryany *et al.* (2008a, 2008b), who were the first to report observations of NIW-associated noise on several HLA hydrophones in the middle of the array.

The third and most intense type of observed noise is illustrated in Fig. 6(d), which uses the SHRU5 data. We interpret this noise type as the noise generated by moving sediments that had been mobilized by the NIW-induced near-bottom currents. After sediment particles leave the seafloor, they generate acoustic waves (noise) by colliding with each other and with the stationary seabed as well as with near-bottom acoustic sensors and/or their housing. Mobilization of sediments and dynamics of the suspended sediment particles are controlled by the composition of surficial sediments and the near-bottom current velocity.

To our knowledge, NIW-induced SGN has not been previously described. [The possibility of the occurrence of such noise was hypothesized by Serebryany *et al.* (2008a) and Yang *et al.* (2015).] However, there is extensive literature on SGN produced by other kinds of currents such as river flow, orbital velocities in surface gravity waves, and tidal currents (Bassett, 2013; Thorne, 2014; Rickenmann, 2017). SGN has been measured using underwater sensors and seismometers on dry land (Roth *et al.*, 2016). SGN properties have been studied in laboratory experiments (Thorne, 1985, 1986) and in rivers (Roth *et al.*, 2016; Geay *et al.*, 2017; Petrut *et al.*, 2018) as well as in straits (Thorne, 1986; Bassett, 2013) and the surf zone at sea (Voulgaris *et al.*, 1999). Bassett *et al.* (2013) investigated SGN caused by currents in a tidal channel in Puget Sound. They found that a near-bottom current velocity above a critical value of 50–60 cm/s was necessary to produce SGN and that the shape of the SGN spectrum depended on sediment grain size. SGN was typically most pronounced above 2 kHz with a maximum spectral density at frequencies of 10–15 kHz.

The threshold character, frequency content, and value of the current velocity threshold (Sec. III) of the type-three NIW-induced noise are consistent with the previously observed SGN due to tidal currents in the ocean, which supports our interpretation of the mechanisms of the type-three noise. The difference in the current velocity thresholds (~40 cm/s vs 50–60 cm/s) can be attributed to a difference in the sediment grain sizes at the experiment sites on the New Jersey shelf and in Puget Sound.

Let us compare quantitatively the conditions, under which the third noise type was observed, with the conditions (e.g., Miller *et al.*, 1977; Wiberg and Smith, 1987) needed for sediment mobilization to occur at the SW'06 experiment site. Sediment grains begin to move and SGN arises when the shear stress due to near-bottom current exceeds a certain threshold. The shear stress and the threshold (critical) shear stress are usually characterized in terms of the shear, or friction, velocity u_* and its critical value u_*^{cr}. Experimentally determined dependence of u_*^{cr} on the grain size D of well-sorted, siliciclastic sediments (the Inman curve) can be found in Miller *et al.* (1977) and, with additional experimental results, in Wiberg and Smith (1987). It is reproduced in Fig. 7(a) (curve 5). A semi-empirical theory of the critical shear stress is presented by Wiberg and Smith (1987) for sediments consisting of either grains of the same size or a mixture of grains of different sizes. The seabed roughness, which affects the turbulent flow in the near-bottom boundary layer, is characterized in this theory by the roughness scale length k_s. For well-sorted (uniform) sediments, $k_s = D$;

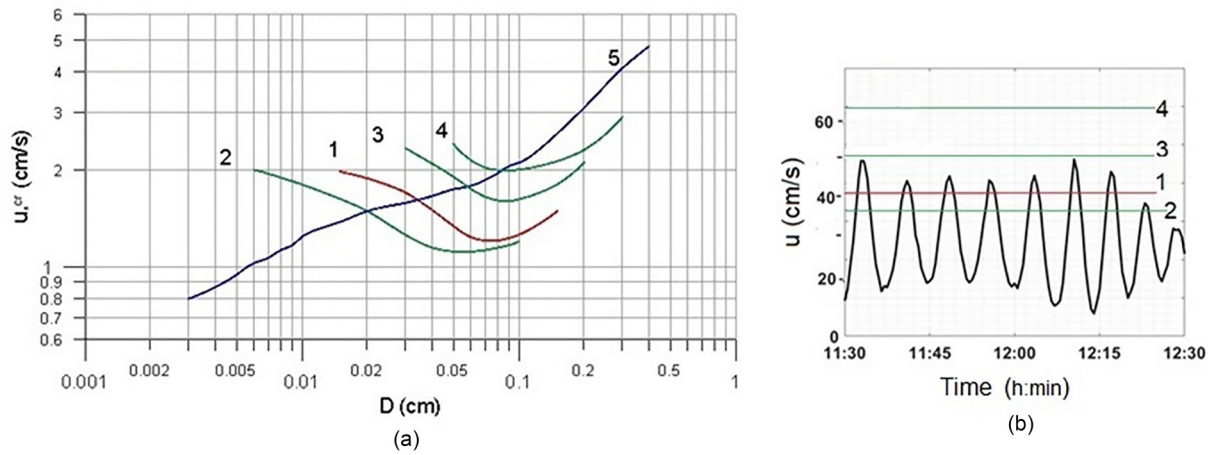

FIG. 7. (Color online) Theoretical estimates of the threshold of sediment mobilization by near-bottom currents. (a) The minimum value u_*^{cr} of the shear velocity u_* that leads to mobilization of sediment grains of size D is depicted under the conditions of the SW'06 experiment, where $k_s = 0.035$ cm (1), and for seabeds with three other roughness scales: $k_s = 0.02$ cm (2), 0.07 cm (3), and 0.10 cm (4). The threshold u_*^{cr} values are calculated following Wiberg and Smith (1987). Also shown is the Inman curve (5), which gives an experimentally determined u_*^{cr} for well-sorted seabeds with $k_s = D$. The Inman curve is adapted from Miller *et al.* (1977) and Wiberg and Smith (1987). (b) ADCP-measured time dependence of the horizontal current velocity at depth of 68.3 m. Thin horizontal lines show theoretical values of the minimum current velocity required for mobilization of the poorly sorted sediments of the four different sediment types considered in (a). Time (GMT) on 19 August 2006 is shown in hours and minutes.

https://doi.org/10.1121/10.0003624

for poorly sorted sediments, which contain a range of grain sizes, k_s can be evaluated as the 65th percentile, D_{65}, of the grain size distribution (Wiberg and Smith, 1987). In poorly sorted sediments, mobilization conditions are different for grains of different size. Lines 1–4 in Fig. 7(a) show the threshold shear velocities u_*^{cr} vs the grain size D for several values of the seabed roughness scale k_s. These curves are calculated as a product of the u_*^{cr} value at $D = k_s$, which is given by the Inman curve, and the square root of the theoretically predicted ratio of the critical shear stresses at a given value of the ratio D/k_s and at $D/k_s = 1$. The shear stress ratio had been calculated by Wiberg and Smith (1987) as a function of the critical roughness Reynolds number $u_*^{cr}k_s/\nu$, where ν is the kinematic viscosity of water, for a discrete set of D/k_s values and was taken from Fig. 7 in Wiberg and Smith (1987). Note that u_*^{cr} increases monotonically with increasing D, when $D = k_s$ [see the Inman curve (curve 5) in Fig. 7(a)], and decreases when the ratio D/k_s increases (Wiberg and Smith, 1987). For each fixed roughness scale, in the range of k_s values represented in Fig. 7(a), the product of the steadily increasing and the steadily decreasing function of grain size D results in the dependence of u_*^{cr} on D, to be referred to as a modified Inman curve, which has a minimum at a certain grain size [see curves 1–4 in Fig. 7(a)]. The minimum value is less than the value at the point $D = k_s$, where the modified Inman curve and the Inman curve intersect. Hence, mobilization of the poorly sorted seabed starts at a smaller current velocity than of a well-sorted seabed with the same roughness scale.

Assuming the theory of Wiberg and Smith (1987) applies to a mixture of grains with a wide range of sizes, the modified Inman curves in Fig. 7(a) indicate that poorly sorted sediments become mobilized when the shear velocity of the near-bottom current exceeds the minimum of the modified Inman curve calculated for the roughness scale k_s of that particular seabed. Only grains with the size that minimizes the respective modified Inman curve are mobilized at first; mobilization of grains in an increasingly wider range of D values occurs when u_* rises further above its minimum on the modified Inman curve.

Sediment material properties on the New Jersey shelf, including the SW'06 site, have been investigated by Goff *et al.* (2004). With respect to locations of our acoustic and current velocity measurements, the two closest points, where grab samples were taken by Goff *et al.* (2004), are at 73.07922°N, 39.04995°W and 73.05421°N, 39.03689°W. These points are within 2 km of where the acoustic and current velocity data illustrated in Figs. 3(a) and 3(d) were obtained. The seafloor sediments are siliciclastic, and their size distribution was classified by Goff *et al.* (2004) as "high fine/low coarse." A representative histogram of the size distribution for this sediment type is given in Fig. 3 in Goff *et al.* (2004). The size distribution is rather broad. The histogram peaks between 250 and 375 μm, with the average grain size of 293 μm and 20.1% and 1.1% by weight, respectively, of the fine ($D < 63$ μm) and coarse ($D > 4000$ μm) grains. We used the histogram to find $D_{65} \approx 350$ μm.

To relate the theoretical conditions of the onset of sediment motion to observed NIWs, we utilize the ADCP current measurements [Fig. 3(d)] at the largest available depth of 68.3 m, or 17.7 m above the seabed. Line 1 in Fig. 7(b) depicts the modified Inman curve for the seabed roughness scale $k_s = D_{65} = 0.035$ cm expected at the sites of the SHRU3 and ADCP measurements that are shown in Figs. 3(a) and 3(d). At elevations z above the seabed, which are much larger than k_s, the flow velocity profile in the boundary layer is logarithmic,

$$u(z) = \kappa^{-1}u_* \ln\left(\frac{z}{z_0}\right), \tag{5}$$

where von Karman's constant is $\kappa = 0.407$, and $z_0 = k_s/30$ (Wiberg and Smith, 1987).

To verify that the logarithmic velocity profile model is appropriate at the depths where the ADCP data is available, we followed Lueck and Lu (1997) and Bassett *et al.* (2013) and characterized the accuracy of the logarithmic regression of the measurements up to different elevations above the seabed in terms of the coefficient of determination R^2. Measured horizontal current velocity profiles during the NIW passage on 19 August 2006 (Fig. 3) were retrieved with 30 s intervals. The ADCP measurements with horizontal current velocity of at least 35 cm/s at the deepest point were selected for analysis. These measurements correspond to time intervals around the time of passage of peaks of soliton-like waves and include all the times when sediment mobilization by NIWs was expected to occur. The logarithmic approximation was found to be applicable up to 30–35 m above the seabed, with $R^2 > 0.8$ for all current velocity profiles and $R^2 > 0.9$ for 88% of the measurements. Larger R^2 typically corresponded to stronger currents.

Equation (5) was used to relate the minima of the threshold values u_*^{cr} in Fig. 7(a), which are equal to 1.2, 1.1, 1.6, and 2.0 cm/s on lines 1–4, respectively, to corresponding current velocities of 40, 38, 52, and 63 cm/s at a depth of 68.3 m in Fig. 7(b). The sediment at the SHRU3 site is expected to become mobilized when the measured current velocity reaches 40 cm/s. This condition is met for the first seven soliton-like waves in the NIW in Fig. 7(b). Grains with sizes between 700 and 800 μm will be mobilized first [see line 1 in Fig. 7(a)]. Such grains are present at a considerable level in the measured size distribution in Goff *et al.* (2004). As the current velocity increases to 50 cm/s in the first soliton-like wave, the mobilization threshold u_*^{cr} is exceeded in a wider range of the grain sizes [Fig. 7(a)], which includes a part of the maximum of the size distribution at $D > 350$ μm.

Figure 3(a) shows six periods of the type-three noise occurrence at SHRU3 rather than the seven peaks predicted based on the ADCP measurements. As has been discussed in Sec. III, the difference between the number of the strong peaks in the current velocity [Fig. 3(d)] and acoustic [Fig. 3(a)] measurements can be attributed to the NIW train evolution on its path from the ADCP to SHRU3.

The predictions of sediment mobilization by the NIW are rather sensitive to the grain size distribution. For coarser sediments with a seabed roughness length of 0.070 or 0.100 cm instead of $k_s = 0.035$ cm derived from the Goff *et al.* (2004) measurements, the observed NIW-induced currents are not strong enough to mobilize the sediments [Fig. 7(b)]. In contrast, if sediments were finer and had $k_s = 0.020$ cm, it would increase the number of soliton-like waves in the observed NIW train that mobilize that sediments [see line 1 in Fig. 7(b)]. If the sediments had the same mean grain size of 293 μm as at the SW'06 site but were well-sorted, an estimate of u_*^{cr} from the Inman curve gives the critical current velocity of 55 cm/s at depth of 68.3 m, which exceeds the NIW-induced currents in Fig. 7(b). Hence, no sediment mobilization would occur in that case.

Because of the uncertainties in the knowledge of the sediment properties at the exact site of acoustic observations and current measurements, due to SHRU 3 and the ADCP not being co-located, and because of the assumptions and approximations inherent to the Wiberg and Smith theory, the derived value of 40 cm/s for the threshold current velocity should be viewed as an estimate rather than an accurate prediction. Nevertheless, the close agreement between the model of the onset of sediment mobilization and acoustic observations of the emergence and disappearance of the type-three noise is remarkable. The quantitative agreement between the conditions of the occurrence of the type-three acoustic noise and the sediment entrainment strongly supports our interpretation of this noise type as SGN.

Figure 8 compares power spectra and intensity of the NIW-induced noise on three hydrophones, where one of the three noise types dominates. We used the data obtained with SHRU5, one VLA hydrophone, and one HLA hydrophone. These are the same sensors that were used in Fig. 6 to illustrate the differences between the three noise types. Power spectra of the background ambient noise are usually modeled using the well-known Wenz curves (Wenz, 1962). When there were no NIWs in the vicinity of the sensors, all three hydrophones recorded signals with rather similar spectra at all frequencies above 10 Hz [Fig. 8(a)]. The measured spectra were close to the Wenz curve if contributions of the spectral peaks due to linear frequency modulated signals around 300 and 500 Hz and other signals emitted by known research sound sources are excluded (Newhall *et al.*, 2007; Lynch and Tang, 2008).

In the presence of a NIW train [Fig. 8(b)], the spectrum of the acoustic pressure on the VLA hydrophone did not change appreciably, except at frequencies below 10 Hz. This is consistent with the flow noise properties. Signals from the research sources could still be clearly seen above the noise background. In contrast, very strong, broadband increase of noise level [Fig. 8(b)] occurred on HLA, which was dragged along the seafloor by the NIW-induced current. The spectrum retained manifestations of the research sources in the 300–1000 Hz frequency band. At SHRU5, where the velocity of the NIW-induced near-bottom current exceeded the threshold for type-three noise generation, there was a broadband increase of the spectral level of about 30 dB between 10 Hz and 2 kHz and a rather sharp increase of the spectral level (up to ~40–50 dB relative to the background noise level) at frequencies above 2 kHz [Fig. 8(b)]. The spectral maximum occurred at frequencies above the highest frequency that can be resolved with the 9765.625 Hz sampling rate of the SHRU5 measurements, as expected for SGN (Thorne, 1986; Bassett *et al.*, 2013; Petrut *et al.*, 2018). At SHRU5, NIW-induced SGN surpassed contributions of all other sources of sound at every frequency.

The increase due to type-three noise in the spectral level of the sound observed at SHRU5 (Fig. 8) is larger and extends to lower frequencies than in other oceanic observations reported by Thorne (1986) and Bassett *et al.* (2013) for comparable and even stronger near-bottom currents. SGN intensity is often considered to be a measure of sediment transport rates (Thorne, 1986, 2014; Voulgaris *et al.*, 1999) for a given sediment and instrument type. However, it is harder to compare SGN levels created by different

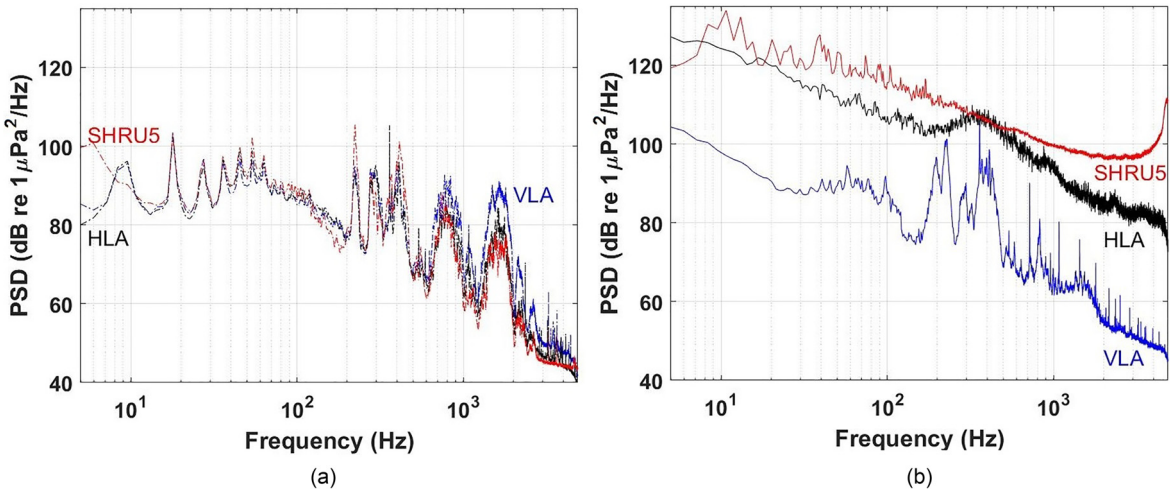

FIG. 8. (Color online) Power spectra of acoustic pressure recorded by SHRU5 and hydrophones on vertical and horizontal arrays when NIWs are absent (a) or present (b). The power spectra are calculated for the same hydrophones as in Fig. 6.

https://doi.org/10.1121/10.0003624

sediments and measured by dissimilar instruments. Noise at SHRU5 may have been enhanced by the vertical advection of entrained sediment particles by NIW currents or by direct impacts of these particles on the hydrophone or elements of the mooring. Furthermore, the sharp increase in the noise spectral level at the highest resolved frequencies and extension of the type-three noise well below 1 kHz [Fig. 8(b)] suggest the possibility of aliasing of higher-frequency SGN energy into the observation band. These possible contributions to the observed noise spectrum can be neither excluded nor quantified with the available SW'06 data. In view of these uncertainties as well as significant differences in the sediment composition between different sites, the larger effect of sediment mobilization on noise spectral levels at SHRU5 than in the previous observations (Thorne, 1986; Bassett *et al.*, 2013) should not be interpreted to mean that the NIW-induced sediment transport on continental shelf is stronger than the sediment transport in tidal channels.

V. DISCUSSION

As mentioned in Sec. II, in the 6 weeks of SW'06 acoustic measurements, a few tens of strong NIW trains were detected. During the 6-day period from 17 to 22 August 2006 chosen for this study, strong NIW trains and attendant noise bursts were observed three more times in addition to the 19 August 2006 event analyzed above. A particularly large NIW train, which contained 11 soliton-like waves with large amplitudes, occurred at nighttime on 17–18 August 2006. The noise bursts generated by this wave train were registered on SHRU3, SHRU4, and SHRU5 with the acoustic intensity and spectrograms rather similar to those measured on 19 August. Weaker NIW trains, with only three prominent soliton-like waves, which were of smaller amplitude, were observed on 18 and 22 August. The noise bursts accompanying these NIW trains were detected on SHRU4 and SHRU5 but not SHRU3 and had lower acoustic intensity than on 19 August. The spectrograms of the noise bursts observed by the SHRUs during the three NIW events revealed contributions of the low-frequency type-one, or flow, noise and the high-frequency type-three noise, which we interpret as SGN.

SGN is an acoustic manifestation of sediment mobilization by water flow. While NIW-induced SGN apparently has not been studied previously, there exists a large body of work on the effects that NIWs have on marine sediments on the continental shelf, and there is no doubt that sediment mobilization by NIWs does occur. It is known that the boundary layer at the footprint of NIW can became hydrodynamically unstable, and this instability results in an increase of the sediment resuspension rate (Carr and Davies, 2006). Moreover, any increase in the turbulent energy due to the hydrodynamic instability can maintain a higher sediment concentration in the water column. Bogucki *et al.* (1997) reported observations and analysis of the sediment resuspension/saltation produced by NIWs on the Californian continental shelf. Quaresma *et al.* (2007) studied sediment resuspension by NIWs using data obtained on the Portuguese continental shelf, where the bathymetry and sound speed profile are similar to those at the SW'06 site. It was shown that water turbidity and the concentration of entrained sediment particles in the water changed synchronously with the thermocline displacement. During the maximum thermocline displacement near the leading front of a NIW train, sediment grains were found as far as 35 m from the seafloor. Another example of strong variations in water turbidity due to sediment resuspension by NIWs and formation of an intermediate nepheloid layer was reported by Masunaga *et al.* (2015). Observations of NIW-induced sediment resuspension are supported by theory and by the results of numerical simulations (Cacchione and Southard, 1974; Bogucki and Redekopp, 1999; Stastna and Lamb, 2008; Olsthoorn and Stastna, 2014; Bourgault *et al.*, 2014).

SGN theory, modeling, and experimental data are reviewed by Bassett *et al.* (2013) and Thorne (2014). SGN theory is based on a model of collisions between two sediment particles or between a particle with a slab (obstacle) (Thorne and Foden, 1988; Bassett *et al.*, 2013; Thorne, 2014). The spectrum of the radiated sound has a maximum, and the centroid frequency of SGN $f_r \approx C/D^{0.9}$, where D is an effective diameter of sediment particles and C is a function of their material properties (Thorne, 1986; Bassett *et al.*, 2013). For instance, $f_r > 45$ kHz for siliciclastic particles with diameters in the 350–1750 μm range, which are expected to be mobilized at the SHRU3 site. This should not be interpreted to mean, however, that the SGN spectrum is concentrated around the centroid frequency or vanishes in the frequency band of our observations. SGN is very broadband and extends to frequencies orders of magnitude below the centroid frequency f_r. An example of existence of significant low-frequency components of SGN is provided by seismic measurements of sediment transport in rivers. Roth *et al.* (2016) infer sediment transport from seismic SGN in the 5–100 Hz frequency band for sediments with $D_{50} = 8$ cm. The centroid frequency estimates (Thorne, 2014; Bassett *et al.*, 2013) would require 25–30 m "particles" to explain 10 Hz noise.

Collisions of two suspended sediment particles are the best-studied (Thorne and Foden, 1988; Thorne, 2014) but not the only source of SGN. Cascades of momentum transfer between several sediment particles, which were documented by Bassett *et al.* (2013), occur on longer time scales than a collision of two particles and, therefore, generate lower-frequency sound (Thorne and Foden, 1988). Impact of a particle on the seabed creates the force chains, which extend in unconsolidated sediments to a depth of many particle radii. Such an impact takes a much longer time than a two-particle collision (Krizou and Clark, 2020) and creates a longer-living acoustic source, thus generating lower-frequency components of SGN.

Laboratory measurements of SGN spectrum support the field observations of SGN at frequencies much lower than its centroid frequency [see Thorne (1985, 1986) and Thorne and Foden (1988)]. For instance, Fig. 6(b) in the review

paper by Thorne (2014) shows a long low-frequency tail of the measured SGN spectrum for 750- and 1500-μm particles. The tail is much heavier than predicted by the Thorne and Foden (1988) theory. For 1500-μm particles, PSD at 10 kHz decreases by only 4.8 dB from the PSD peak value at about 50 kHz. The low-frequency noise is even more pronounced for the smaller, 750-μm particles, with the PSD decreasing by only 3.7 dB between the peak at 100 kHz and 10 kHz. Thus, results of laboratory measurements indicate that strong SGN is expected to be generated at SHRU3 and SHRU5 locations in the frequency band of our field measurements.

Acoustic intensity of SGN increases with current velocity and was found to be an acceptable proxy for bedload transport (Thorne, 2014). Recording and analyzing SGN can serve as minimally invasive, continuous means of measurement for sediment transport and for estimating dimensions of mobile particles (Thorne, 2014). This approach was applied to study sediment transport by various types of water flow, including rivers, tidal currents in straits, and surface gravity wave-induced flows in the surf zone (Thorne, 1986; Mason *et al.*, 2007; Thorne, 2014; Geay *et al.*, 2017; Rickenmann, 2017; Petrut *et al.*, 2018). Results of SGN analysis, including estimates of grain size distribution, agree well with the direct sampling methods (Petrut *et al.*, 2018). Observations of NIW-induced noise bursts and identification of SGN as a dominant contribution to their intensity on near-bottom sensors raise the possibility of extending the passive acoustic measurements of sediment transport to the sediment mobilization by strong NIWs on continental shelves. The inherent ability of the technique to provide long-term series of autonomous observations is even more important on continental shelves than for measurements in rivers or in the surf zone. Moreover, measurements of the noise bursts with autonomous, moored, single-hydrophone receivers can potentially contribute to improved quantitative understanding of NIW-induced near-bottom currents as well as NIW amplitudes and their temporal and spatial variability on the continental shelf.

SGN has an ambient component, which results from sediment particles' collisions with each other and the seabed, as well as a sensor-related component due to particle impacts on the acoustic sensor or its housing. Observations of sediment transport in rivers with sensors on dry land (Roth *et al.*, 2016) offer clear evidence of the ambient component of SGN. On the other hand, sensors are routinely augmented by pipes and plates to increase particle impacts for the purposes of measuring coarse gravel transport (Thorne, 2014; Rickenmann, 2017). Further research is needed to quantify the relative weight of the ambient and sensor-related components of SGN in the NIW-generated noise bursts and the variation of the weight with distance to the seafloor.

Given its high intensity, NIW-induced SGN may present significant challenges for the continuous operation of near-bottom acoustic sensors deployed for underwater communication, detection, and tracking of biological or man-made sound sources or remote sensing of the water column and seabed properties. SGN would be equally detrimental whether ambient or sensor-related. Spectral and spatial characteristics of the NIW-induced noise need to be understood and considered during design and deployment of acoustic systems on continental shelves.

In the context of acoustic phenomena associated with the sediment mobilization by NIWs, SW'06 observations have a number of limitations, which make an unambiguous identification of noise generation mechanisms challenging, lessen somewhat the confidence in our interpretation of the type-three noise as SGN, and call for a dedicated field experiment. The key limitations of the dataset underlying our analysis are the lack of independent measurements of sediment transport or water turbidity to verify sediment mobilization, unavailability of current velocity measurements near the seabed at the exact locations of SHRUs, and absence of high-frequency acoustic measurements encompassing the peak of the SGN spectrum. These limitations emerged, in part, because neither the occurrence of NIW-induced noise bursts nor SGN generation by NIWs were anticipated at the time of the SW'06 experiment.

Our results and the above discussion suggest that a dedicated experiment to unambiguously and more fully characterize the NIW-induced SGN on the continental shelf should include contact measurements of sediment properties and sediment transport, a high-frequency ADCP for high-resolution measurements of the current velocity profile as close as a meter or a few meters from the seabed, and acoustic measurements in an extremely broad frequency band from about 1 Hz to above 100 kHz. The sediment, flow velocity, and acoustic measurements should be collocated and conducted at a site where sediment mobilization by NIWs is expected to occur according to the Wiberg and Smith (1987) model or a similar model. To distinguish between and separately characterize the ambient and instrument-related components of SGN, one can either simultaneously deploy hydrophones with and without a soft cover, which prevents impacts of sediment particles on the sensor and the mooring, or measure the noise spectrum on a vertical hydrophone array extending from the seabed to beyond the layer with suspended sediment particles.

VI. CONCLUSIONS

In this study, we used a network of temperature, current velocity, and acoustic sensors deployed on the continental shelf off New Jersey to relate the occurrence of large, transient increases in acoustic noise intensity (noise bursts) to trains of strongly nonlinear internal waves and, more specifically, to individual localized, soliton-like waves that form the trains. The noise bursts occurred in sequences of 60–80 min, the duration of which equals the time it took a NIW train to travel past an observation point on the New Jersey shelf. Individual noise bursts lasted for 5–7 min and coincided in time with passage of a single soliton-like internal wave past the hydrophone. Very large increases in the

spectral density and broadband intensity of noise, of up to 50 dB relative to background, were observed on hydrophones located 6–7 m above the seafloor. The peak acoustic intensity and the spectral content of the noise bursts were controlled by the amplitude of individual soliton-like internal waves and were most directly related to the velocity of the NIW-induced near-bottom currents.

The noise burst emergence and observed variations in their intensity and spectral content with water depth, hydrophone elevation above the seafloor, and NIW amplitude have been tentatively explained in terms of three noise generation mechanisms. The low-frequency (below a few tens of Hertz) component of the noise bursts represents the flow noise that occurs due to advection of turbulent pressure pulsations past an acoustic sensor. Hydrophones lying on the seafloor recorded broadband noise, which resulted from the hydrophones being dragged along the seafloor by NIW-induced currents. The strongest noise bursts were associated with sediment generated noise (SGN). Acoustic waves are generated when sediment is mobilized by NIW currents and sediment particles collide with each other, with the stationary seabed, and with acoustic sensors. SGN was most pronounced at frequencies above 2 kHz. A distinctive feature of SGN is its threshold character. NIW-induced near-bottom currents stronger than about 40 cm/s were found to be necessary to initiate SGN. Compared to previously described oceanic observations of SGN in tidal channels and the near-shore surf zone, NIW-induced SGN occurs on the continental shelf at significantly larger water depths than most previous observations and drastically increases the extent of the seafloor area where SGN occurrence should be expected.

NIW-generated noise bursts are one of the strongest reported acoustic effects of internal waves in the ocean. The noise bursts may present challenges to continuous acoustic communication and acoustic monitoring of the ocean using near-bottom sensors. On the other hand, measurements of the noise bursts with autonomous, single-hydrophone receivers can potentially contribute to improved quantitative understanding of NIW-induced near-bottom currents and sediment transport by internal waves on the continental shelf. Further research, including dedicated field experiments, is needed to fully characterize the spectrum of NIW-induced acoustic noise, its depth dependence, relative contributions of the ambient and sensor-related components of SGN, and the directivity and correlation properties of the ambient component of the NIW-generated acoustic noise.

ACKNOWLEDGMENTS

The authors are grateful to A. Serebryany and an anonymous reviewer for their valuable comments, which helped us improve the manuscript. The SW'06 experiment was supported by the United States Office of Naval Research. The data used in this study were collected by the Woods Hole Oceanographic Institution (2006). This work was supported by National Science Foundation Grant No. OCE1657430, Binational Science Foundation Grant No. 2016545, Office of Naval Research (ONR) Award No. N00014-20-WX01312, and ONR Global Grant No. N62909-16-1-2079-P00002.

Apel, J. (**2003**). "A new analytical model for internal solitons in the ocean," J. Phys. Oceanogr. **33**, 2247–2268.
Apel, J. R., Ostrovsky, L. A., Stepanyants, Y. A., and Lynch, J. F. (**2007**). "Internal solitons in the ocean and their effect on underwater sound," J. Acoust. Soc. Am. **121**(2), 695–722.
Badiey, M., Katsnelson, B. G., Lynch, J. F., and Pereselkov, S. (**2007**). "Frequency dependence and intensity fluctuations due to shallow water internal waves," J. Acoust. Soc. Am. **122**(2), 747–760.
Badiey, M., Mu, Y., Lynch, J., Apel, J., and Wolf, S. (**2002**). "Temporal and azimuthal dependence of sound propagation in shallow water with internal waves," IEEE J. Oceanic Eng. **27**(1), 117–129.
Bassett, C., Thomson, J., Dahl, P. H., and Polagye, B. (**2014**). "Flow-noise and turbulence in two tidal channels," J. Acoust. Soc. Am. **135**(4), 1764–1774.
Bassett, C., Thomson, J., and Polagye, B. L. (**2013**). "Sediment-generated noise and bed stress in a tidal channel," J. Geophys. Res. Oceans **118**(4), 2249–2265, https://doi.org/10.1002/jgrc.20169.
Bogucki, D., Dickey, T., and Redekopp, L. G. (**1997**). "Sediment resuspension and mixing by resonantly generated internal solitary waves," J. Phys. Oceanogr. **27**(7), 1181–1196.
Bogucki, D., and Redekopp, L. (**1999**). "A mechanism for sediment resuspension by internal solitary waves," Geophys. Res. Lett. **26**(9), 1317–1320, https://doi.org/10.1029/1999GL900234.
Bourgault, D., Morsilli, M., Richards, C., Neumeier, U., and Kelley, D. E. (**2014**). "Sediment resuspension and nepheloid layers induced by long internal solitary waves shoaling orthogonally on uniform slopes," Cont. Shelf Res. **72**, 21–33.
Cacchione, D. A., and Southard, J. B. (**1974**). "Incipient sediment movement by shoaling internal gravity waves," J. Geophys. Res. **79**(15), 2237–2242, https://doi.org/10.1029/JC079i015p02237.
Carr, M., and Davies, P. A. (**2006**). "The motion of an internal solitary wave of depression over a fixed bottom boundary in a shallow, two-layer fluid," Phys. Fluids **18**, 016601.
Colosi, J. A., Scheer, E. K., Flatté, S. M., Cornuelle, B. D., Dzieciuch, M. A., Munk, W. H., Worcester, P. F., Howe, B. M., Mercer, J. A., Spindel, R. C., and Metzger, K. (**1999**). "Comparisons of measured and predicted acoustic fluctuations for a 3250-km propagation experiment in the eastern North Pacific Ocean," J. Acoust. Soc. Am. **105**(6), 3202–3218.
Geay, T., Belleudy, P., Gervaise, C., Habersack, H., Aigner, J., Kreisler, A., Seitz H., and Laronne, J. (**2017**). "Passive acoustic monitoring of bed load discharge in a large gravel bed river," J. Geophys. Res. Earth Surface **122**(2), 528–545.
Godin, O. A., Voronovich, A. G., and Goncharov, V. V. (**2006**). "Refraction of sound in a horizontally inhomogeneous, time dependent ocean," IEEE J. Oceanic Eng. **31**(2), 384–401.
Goff, J. A., Kraft, B. J., Mayer, L. A., Schock, S. G., Sommerfield, C. K., Olson, H. C., Gulick, S. P., and Nordfjord, S. (**2004**). "Seabed characterization on the New Jersey middle and outer shelf: Correlatability and spatial variability of seafloor sediment properties," Mar. Geol. **209**(1–4), 147–172.
Kaiser, J., and Schafer, R. (**1980**). "On the use of the I_0-sinh window for spectrum analysis," IEEE Trans. Acoust. Speech Signal Process. **28**(1), 105–107.
Katsnelson, B. G., Grigorev, V., Badiey, M., and Lynch, J. F. (**2009**). "Temporal sound field fluctuations in the presence of internal solitary waves in shallow water," J. Acoust. Soc. Am. **126**(1), EL41–EL48.
Krizou, N., and Clark, A. H. (**2020**). "Power-law scaling of early-stage forces during granular impact," Phys. Rev. Lett. **124**(17), 178002.
Linder, C. A., and Gawarkiewicz, G. (**1998**). "A climatology of the shelf-break front in the Middle Atlantic Bight," J. Geophys. Res. Oceans **103**, 18405–18423, https://doi.org/10.1029/98JC01438.
Lueck, R. G., and Lu, Y. (**1997**). "The logarithmic layer in a tidal channel," Cont. Shelf Res. **17**(14), 1785–1801.
Lynch, J., and Tang, D. (**2008**). "Overview of Shallow Water 2006 JASA EL Special Issue Papers," J. Acoust. Soc. Am. **124**(3), EL63–EL65.
Mason T., Priestley D., and Reeve, D. E. (**2007**). "Monitoring near-shore shingle transport under waves using a passive acoustic technique," J. Acoust. Soc. Am. **122**(2), 737–746.

Masunaga, E., Homma, H., Yamazaki, H., Fringer, O. B., Nagai, T., Kitade, Y., and Okayasu, A. (**2015**). "Mixing and sediment resuspension associated with internal bores in a shallow bay," Cont. Shelf Res. **110**, 85–99.
Miller, M. C., McCave, I. N., and Komar, P. (**1977**). "Threshold of sediment motion under unidirectional currents," Sedimentology **24**(4), 507–527.
Newhall, A. E., Duda, T. F., von der Heydt, K., Irish, J. D., Kemp, J. N., Lerner, S. A., Liberatore, S. P., Lin, Y. T., Lynch, J. F., and Maffei, A. R. (**2007**). "Acoustic and oceanographic observations and configuration information for the WHOI moorings from the SW06 experiment," Technical Report No. WHOI-2007-04 (Woods Hole Oceanographic Institution, Falmouth, MA).
Newhall, A. E., Lin, Y.-T., Lynch, J. F., Baumgartner, M. F., and Gawarkiewicz, G. G. (**2012**). "Long distance passive localization of vocalizing sei whales using an acoustic normal mode approach," J. Acoust. Soc. Am. **131**(2), 1814–1825.
Olsthoorn, J., and Stastna, M. (**2014**). "Numerical investigation of internal wave-induced sediment motion: Resuspension versus entrainment," Geophys. Res. Lett. **41**(8), 2876–2882, https://doi.org/10.1002/2014GL059826.
Petrut, T., Geay, T., Gervaise, C., Belleudy, P., and Zanker, S. (**2018**). "Passive acoustic measurement of bedload grain size distribution using self-generated noise," Hydrol. Earth Syst. Sci. **22**(1), 767–787.
Quaresma, L. S., Vitorino, J., Oliveira, A., and da Silva, J. (**2007**). "Evidence of sediment resuspension by nonlinear internal waves on the western Portuguese mid-shelf," Mar. Geol. **246**(2), 123–143.
Rickenmann, D. (**2017**). "Bed-load transport measurements with geophones and other passive acoustic methods," J. Hydraulic Eng. **143**(6), 03117004.
Roth, D. L., Brodsky, E. E., Finnegan, N. J., Rickenmann, D., Turowski, J. M., and Badoux, A. (**2016**). "Bed load sediment transport inferred from seismic signals near a river," J. Geophys. Res. Earth Surface **121**(4), 725–747, https://doi.org/10.1002/2015JF003782.
Serebryany, A. N., Furduev, A. V., Aredov, A. A., and Okhrimenko, N. N. (**2005**). "Ambient noise generated by large-amplitude internal waves in the ocean," Doklady Earth Sci. **402**(4), 654–657.
Serebryany, A., Lynch, J., and Newhall, A. (**2008a**). "Underwater noise generation by nonlinear internal waves on the Atlantic shelf of USA during the experiment 'SHALLOW WATER 2006'," Proc. Russian Acoust. Soc. **9**, 217–227.
Serebryany, A. N., Newhall, A., and Lynch, J. F. (**2008b**). "Observations of noise generated by nonlinear internal waves on the continental shelf during the SW06 experiment," J. Acoust. Soc. Am. **123**(5), 3589–3589.
Shroyer, E. L., Moum, J. N., and Nash, J. D. (**2009**). "Observations of polarity reversal in shoaling nonlinear internal waves," J. Phys. Oceanogr. **39**(3), 691–701.
Shroyer, E. L., Moum, J. N., and Nash, J. D. (**2011**). "Nonlinear internal waves over New Jersey's continental shelf," J. Geophys. Res. Oceans **116**, C03022, https://doi.org/10.1029/2010JC006332.
Simmen, J., Flatté, S. M., and Wang, G. Y. (**1997**). "Wavefront folding, chaos, and diffraction for sound propagation through ocean internal waves," J. Acoust. Soc. Am. **102**(1), 239–255.
Stastna, M., and Lamb, K. G. (**2008**). "Sediment resuspension mechanisms associated with internal waves in coastal waters," J. Geophys. Res. Oceans **113**(C10), C10016, https://doi.org/10.1029/2007JC004711.
Strasberg, M. (**1979**). "Nonacoustic noise interference in measurements of infrasonic ambient noise," J. Acoust. Soc. Am. **66**(5), 1487–1493.
Tang, D., Moum, J. N., Lynch, J. F., Abbot, P., Chapman, R., Dahl, P. H., Duda, T. F., Gawarkiewicz, G., Glenn, S., Goff, J. A., Graber, H., Kemp, J., Maffei, A., Nash, J. D., and Newhall, A. (**2007**). "Shallow Water '06: A joint acoustic propagation/nonlinear internal wave physics experiment," Oceanography **20**(4), 156–167.
Thorne, P. D. (**1985**). "The measurement of acoustic noise generated by moving artificial sediments," J. Acoust. Soc. Am. **78**(3), 1013–1230.
Thorne, P. D. (**1986**). "Laboratory and marine measurements on the acoustic detection of sediment transport," J. Acoust. Soc. Am. **80**(3), 899–910.
Thorne, P. D. (**2014**). "An overview of underwater sound generated by interparticle collisions and its application to the measurements of coarse sediment bedload transport," Earth Surf. Dyn. **2**(2), 531–543.
Thorne, P. D., and Foden, D. J. (**1988**). "Generation of underwater sound by colliding spheres," J. Acoust. Soc. Am. **84**, 2144–2152.
Voulgaris, G., Workman, M., and Collins, M. B. (**1999**). "Measurement techniques of shingle transport in the nearshore zone," J. Coastal Res. **15**(4), 1030–1039.
Webb, S. C. (**1988**). "Long-period acoustic and seismic measurements and ocean floor currents," IEEE J. Oceanic Eng. **13**(4), 263–270.
Wenz, G. M. (**1962**). "Acoustic ambient noise in the ocean: Spectra and sources," J. Acoust. Soc. Am. **34**(12), 1936–1956.
Wiberg, P. L., and Smith, J. D. (**1987**). "Calculations of the critical shear stress for motion of uniform and heterogeneous sediments," Water Resources Res. **23**(8), 1471–1480.
Woods Hole Oceanographic Institution (**2006**). "Shallow Water Experiment 2006," http://acoustics.whoi.edu/sw06/ (Last viewed 2/4/2021).
Xue, J., Graber, H. C., Romeiser, R, and Lund, B. (**2014**). "Understanding internal wave-wave interaction patterns observed in satellite images of the Mid-Atlantic Bight," IEEE Trans. Geosci. Remote Sens. **52**(6), 3211–3219.
Yang, Y. J., Chan, H. C., Wu, J. C. H., Liang, W. D., Chen, C. F., and Wei, R. C. (**2013**). "Ocean ambient noises modulated by internal solitary waves," in Proceedings of 2013 MTS/IEEE OCEANS-Bergen, June 10–14, Bergen, Norway, pp. 1–4.
Yang, Y. J., Chiu, C. S., Wu, J. C. H., Liang, W. D., Ramp, S. R., Reeder, D. B., and Chen, C. F. (**2015**). "Observations of ambient noises induced by the internal solitary waves on the continental slope of the northern South China Sea: Ambient noises by ISW in SCS," in: OCEANS 2015-Genova, May 18–21, Genova, Italy, pp. 1–4.
Zhou, J. X., Zhang, X. S., and Rogers, P. (**1991**). "Resonant interaction of sound wave with internal solitons in the coastal zone," J. Acoust. Soc. Am. **90**(4), 2042–2054.